Article

Two-Dimensional Device with Light-Controlled Capability for Treatment of Cancer-Relevant Infection Diseases

Yanbing Yang,[§] Bo Zeng,[§] Jing Guo, Yingxue Li, Yujie Yang, and Quan Yuan*

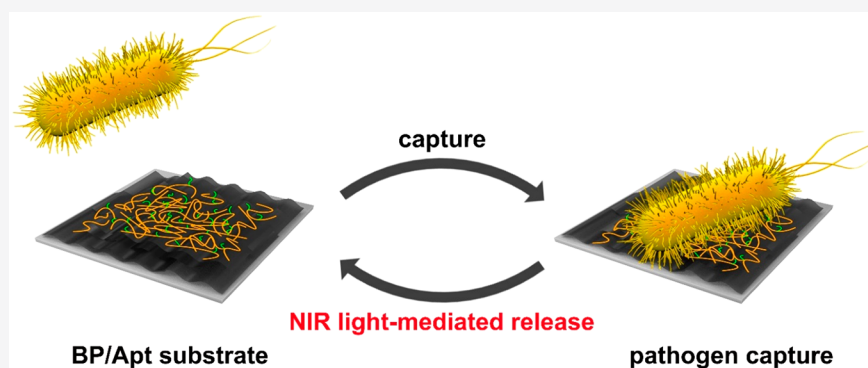Cite This: *Anal. Chem.* 2020, 92, 10162−10168

Read Online

ACCESS | 📊 Metrics & More | 📖 Article Recommendations | 🆂🅸 Supporting Information

ABSTRACT: Concurrent infection in cancer treatment is the leading cause of high cancer mortality that requires urgent action. Currently developed diagnostic methods are hindered by the difficulty of rapidly and reliably screening small amounts of pathogens in the blood and then release pathogens for downstream analysis, limiting the advance of cancer concurrent infection diseases diagnosis and targeted treatment. Herein, we present a near-infrared (NIR) light-responsive black phosphorus (BP)-based device that effectively captures and releases pathogen for downstream drug-resistance analysis. The aptamer-modified BP nanostructures exhibit enhanced topographical interactions and binding capabilities with pathogen, enabling highly efficient and selective capture of pathogen in serum. NIR light irradiation induces BP nanostructure to generate a local thermal effect, which regulates the three-dimensional structure of the aptamer and causes efficient release of pathogen from the substrate surface. The released pathogen is resistant to ampicillin as demonstrated by downstream genetic analysis. The design of the functionalized light-controlled device for monitoring pathogen behavior shows great potential for assisting in cancer therapy and promoting personalized healthcare.

Cancer is one of the most serious chronic diseases and is the leading cause of mortality all over the world. Currently, the most commonly used clinical methods for cancer treatment include chemotherapy and radiotherapy, which can also eliminate lymphocytes at the time for killing cancer cells. Collapse of the autoimmune system significantly suppresses the immune cell-mediated immunity and consequently accelerates the metastasis of cancer cells.[1−9] More importantly, at this period, the foreign microbial could easily attack the host cells and trigger serious whole-body infectious diseases, further increasing the cancer cells diffusion rates and recurrence of disease after surgery treatment.[10−13] Therefore, the high cancer mortality is often due to concurrent infections caused by chemotherapy and radiotherapy. Typically, at the early stages of infection, the empirical broad-spectrum antibiotic therapy is the most commonly used therapeutic strategy, while the broad-spectrum antibiotics fail to treat target-specific pathogens effectively and often lead to the emergence of antibiotic-resistant pathogens.[14−19] In this regard, to realize targeted pathogen treatment, it is critical and necessary to isolate trace amounts of pathogen (1−100 colony-forming units (CFU) mL^{-1}) in the blood and then release the pathogen for downstream drug-resistance analysis at a molecular scale. Currently, research mainly focuses on the development of a functionalized substrate or biochip, such as Si nanowire arrays,[20] polycrystalline NiCo$_2$O$_4$ nanowires,[21] a graphene−silver nanoparticle−silicon sandwich chip,[22] molecules-conjugated silver nanoparticles on a silicon wafer,[23] and hydrogel barcodes,[24] as a candidate for traditional blood culture and polymerase immunoassay to improve the pathogen capture efficiency and capture selectivity as well as reduce the background signal.[20−28] However, the difficulties to rapidly identify pathogenic bacteria as well as release pathogen for downstream genetic analysis are the main barriers to realize
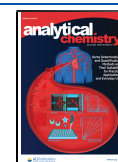
early-stage cancer concurrent infection diseases diagnosis and targeted treatment. Hence, development of a rapid and reliable method to efficiently screen a small amount of pathogens in the blood and then analyze the drug resistance of pathogens to select targeted antibiotic treatment are desirable for assisting in cancer therapy and development of personalized medicine.

To achieve this goal, it would be ideal to design a type of functionalized portable device with the capability of isolating trace amounts of pathogen in the blood through structural and size matching to enhance interfacial topographical interaction as well as the capability of releasing pathogen for downstream analysis. As a fast, simple, and accurate controlling method, light control with the advantages of high spatial and temporal resolution and noninvasive and remote control abilities could activate light-responsive local regions to regulate the structure or behavior of molecules.[29−31] Therefore, it is suggested that a functionalized portable device with light-controlling capability could be developed to enable efficient screening and release of pathogen for downstream genetic analysis.

Thus, here, we construct a near-infrared (NIR) light-responsive device that is based on an aptamer-modified black phosphorus (BP) nanostructure (BP/Apt) for efficient capture as well as controlled release of pathogen in serum for further drug-resistance analysis (Scheme 1). As a kind of layered two-

Scheme 1. Schematic Illustration of the NIR-Responsive BP/Apt Substrate for Capture, Release, and Downstream Genetic Analysis of Pathogen
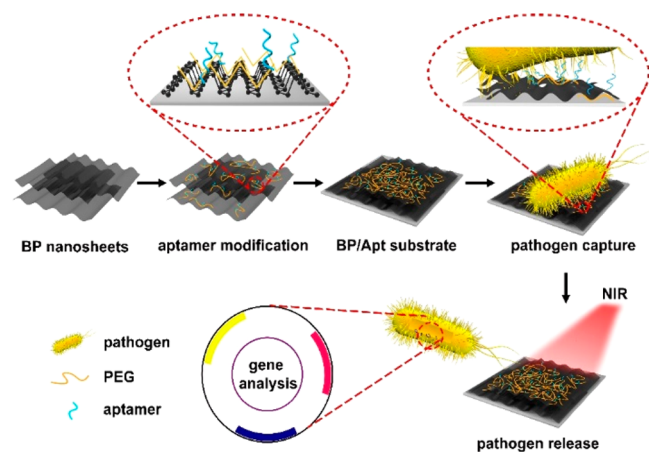
dimensional material, BP exhibits a large surface-to-volume ratio, tunable chemical characteristics, wide spectral absorption, and excellent photothermal properties.[26] The assembled BP nanostructures with rough structure and excellent mechanical flexibility combined with specific DNA aptamer serve as the capture substrate to bind with nanoscaled villi, podia, and nanofibers on cell surfaces through enhanced nanotopography interaction, thereby contributing to highly specific and efficient pathogen capture. Upon NIR light irradiation, the BP nanostructures could absorb the photon energy and produce electron−hole pairs. The photoexcited electrons and holes would release the extra energy to generate heat through nonradiative relaxation. The generated thermal device could regulate the three-dimensional structure of aptamer binding on the BP surface, thus realizing the controlled release of the captured pathogen. Consequently, this optimized aptamer-modified BP nanostructure achieves a significantly improved capture efficiency of 86.0% and release

efficiency of 95.9%. It is also notable that the BP/Apt substrate could identify trace amounts of pathogen down to 10 cells mL^{-1} in serum with a capture efficiency of 60.0%. The downstream genetic analysis of the released pathogen indicates that the pathogen is resistant to ampicillin. It is worth mentioning that this is the first demonstration of a two-dimensional capture and release platform for high-efficiency isolation and release of pathogen in serum for downstream genetic analysis. The design of functionalized substrate for monitoring pathogen behavior offers prospects for assisting in cancer therapy and suggests a general strategy for personalized healthcare. The excellent biocompatibility and biodegradability of BP nanostructures also hold promise to serve as an implantable nanoplatform for in vivo capture of pathogen in blood vessels for clinical applications.

EXPERIMENTAL SECTION

Characterization. The morphological structure of BP-based nanosheets was characterized by SEM (Sigma, Zeiss, Germany), TEM (JEOL JEM 2100), and AFM (Bruker Multimode 8, tapping mode). The UV−vis−NIR absorption spectra of the BP-based substrates were obtained using a UV 2550 spectrophotometer (Shimadzu). The X-ray photo-electron spectra (XPS) were recorded on a Thermo ESCALAB 250Xi spectrometer. Circular dichroism (CD) spectra of aptamer were recorded with a MOS-500 spectrometer. The surface temperature of the BP substrate under 808 nm NIR light irradiation was recorded using a FLIR A35 infrared camera. Raman spectra were measured with Renishaw in Via. Fluorescence microscopy images of the *E. coli* cells were captured on an Axiovert 200M with a 20× objective.

Preparation of BP Nanosheets. The BP nanosheets were obtained by a solvent exfoliation approach according to a previous report.[32−34] Briefly, 200 mg of bulk BP crystals was ground in an Ar glovebox and dispersed in 300 mL of *N*-methyl-2-pyrrolidone. For the exfoliation of BP nanosheets, the resulting mixture dispersion was tip sonicated under anhydrous and Ar gas conditions for 10 h at 100 W power in an ice bath. The ultrasonication probe worked 2 s with an interval of 4 s. Then the as-prepared dispersion was centrifuged at 3000 rpm for 30 min to remove unexfoliated BP crystals. The supernatant was further centrifuged at 7000 rpm for 10 min to isolate precipitate. After washing with ethanol and isopropyl alcohol (IPA), the precipitate was dispersed in IPA for further use.

Functionalization of BP Nanosheets. For the preparation of functionalized BP nanosheets, 10 mg of NH$_2$-PEG-NH$_2$ was first added into 10 mL of a BP nanosheets (200 μg mL^{-1}) dispersion in water. After sonication for 30 min and stirring for 4 h, the obtained amino groups-modified BP nanosheets (BP/PEG) were gathered by centrifugation at 3700 rpm for 30 min and washed with water. Afterward, 300 μg of BP/PEGnanosheets dispersed in 900 μL of PB buffer solution (10 mM, pH value of 7.4) was reacted with 100 μL of sulfosuccinimidyl 4-(*N*-maleimidomethyl) cyclohexane-1-carboxylate (Sulfo-SMCC, 1 mg mL^{-1}) cross-linking reagent for 1 h. By sequentially incubating with 1.3 nmol of *Escherichia coli*-specific aptamer (Apt-*E. coli*) in 865 μL of water overnight at 37 °C and PB buffer rinsing to remove unbound aptamer, the Apt-*E. coli*-modified BP nanosheets were obtained. The *Staphyloccus aureus*-specific apatmer (Apt-*S. aureus*)-modified BP nanosheets were obtained using the same procedure. The

sequences of *E. coli*- and *S. aureus*-specific aptamers are as follows.[35]

Apt-*E. coli*: 5′-ATCC GTCA CACC TGCT CTAC TGGC CGGC TCAG CATG ACTA AGAA GGAA GTTA TGTG GTGT TGGC TCCC GTAT TTT TTT TTT-SH-3′.

Apt-*S. aureus*: 5′-TCC CTA CGG CGC TAA CCC CCC CAG TCC GTC CTC CCA GCC TCA CAC CGC CAC CGT GCT ACA AC TTT TTT TTT-SH-3′.

Fabrication of BP/Apt Substrate. The BP/Apt substrate was fabricated by drop casting the modified BP nanosheets on the patterned glass substrate and then drying the substrate at 30 °C. The polydimethylsiloxane chamber with a 3 mm depth was bonded onto the substrate to form an incubation chamber.

Bacteria Culture. The strains of *E. coli* and *S. aureus* were grown at 37 °C overnight in Luria−Bertani broth medium, which was composed of 0.1 g of peptone, 0.05 g of yeast extract, 0.05 g of NaCl, and 10 mL of water. The bacteria concentration was monitored photometrically by measuring the optical density (OD) at 600 nm. In detail, the bacterial suspensions were diluted to obtain an appropriate OD_{600} value of about 0.1, which corresponds to the CFUs of *E. coli* and *S. aureus* at concentrations of 1×10^8 and 4×10^8 CFU mL^{-1}.

Bacteria Capture and Release. The bacteria capture performance was evaluated by exposing the capture substrate (BP-based and glass-based substrates) into 1 mL of bacteria solution for a period of incubation time. Then the substrate was washed with PB buffer solution three times and dried with nitrogen for fluorescence microscopy observation. The capture efficiency was calculated based on the proportion of bacteria captured in a test bacteria sample. For bacteria release, the substrate with captured bacteria was exposed to NIR light irradiation for 5 min. The surface temperature of the BP/Apt substrate was controlled at 40 °C. The bacteria were released from the BP/Apt substrate due to the conformation change of Apt-*E. coli* or Apt-*S.aureus* upon thermal triggering. The released bacteria were counted with the standard colony counting method to calculate the release efficiency.

SEM Observation of Bacteria on the Substrate Surface. The captured bacteria on the substrate were pretreated for SEM observation. Specifically, the captured bacteria were first fixed with 2.5% glutaraldehyde in PBS for 12 h. Then the bacteria were fixed with 1% osmium tetroxide for 1 h. Tannic acid (1%) was exploited as a mordant. The bacteria were gradient dehydrated with a series of alcohol solutions (15%, 30%, 50%, 70%, 80%, 90%, 100%) followed by freeze drying and platinum deposition for SEM observation.

Capture and Release of Spiked Bacteria from Human Serum Samples. The healthy human serum samples were obtained from Zhongnan Hospital of Wuhan University. The bacteria were spiked into the human serum samples to generate bacteria concentrations of 10, 100, 200, and 500 CFU mL^{-1}. The subsequent capture and release processes are consistent with the experiments performed with bacteria PB dispersions.

Genetic Analysis. Prior to analysis, the bacteria released from the substrate was grown overnight in Luria−Bertani broth medium and collected via centrifugation. Genetic analysis was performed by the Personal Biotechnology Co. (Shanghai, China) using the Illumina Hiseq platform (400 bp inserts library with 2 × 151 bp paired-end sequencing) through Whole Genome Shotgun Sequencing. The antibiotic resistance of *E. coli* was analyzed with the BLAST platform according to the reference sequences of the Comprehensive Antibiotic Resistance Database containing 3008 antibiotic-resistant genes.

■ RESULTS AND DISCUSSION

Construction of BP/Apt Pathogen Capture Platform. To construct a NIR-responsive BP/Apt capture device, the liquid-phase-exfoliated BP nanosheets with lateral dimensions of ~0.4 μm × 3 nm (Figures S1−S3) were first immobilized with amine-polyethylene glycol-amine (NH$_2$-PEG-NH$_2$, 2000 Da) linker molecules by electrostatic interaction, thus introducing amino groups, for conjugating aptamer (Scheme 1). Immobilization of NH$_2$-PEG-NH$_2$ linker molecules on the BP surface was validated by the zeta potential variation (Figure S4, −33.7 mV for BP and −26.4 mV for BP/PEG) due to the positively charged NH$_2$-PEG-NH$_2$ molecules and the presence of N element in the elemental mapping image (Figure S5) of BP/PEG nanosheets. In addition, the thickness of the BP nanosheets increases from 2−4 to 4−6 nm after the NH$_2$-PEG-NH$_2$ functionalization as shown in the atomic force microscopy (AFM) height image (Figure S2). Next, −SH-functionalized aptamer, to capture and preconcentrate the target pathogen, was introduced onto the BP/PEG nanosheets by Sulfo-SMCC cross-linking reagent (Scheme 1). Formation of the C−S bond in the BP/Apt nanosheets and the zeta potential of BP/Apt nanosheets varies to −45.2 mV, suggesting successful binding of −SH aptamer with Sulfo-SMCC (Figures S4 and S6). Then the BP/Apt nanosheets were assembled on the glass surface with a dip-coating strategy to form BP/Apt nanostructures (Scheme 1). The BP/Apt nanostructures not only act as anchors for specific pathogen attachment but also provide NIR light-dependent modulation of the capture or release process. The BP/Apt substrate with a size of 3 mm × 10 mm appears black in color as indicated in the representative photograph of the fabricated BP/Apt substrate (Figure 1a). The scanning electron microscopy (SEM) images of the BP nanostructure (Figure 1b and Figure S7) clearly reveal the rough surface and wrinkled architecture originating from the stacked BP nanosheets, which facilitates the intimate interaction between BP capture substrate and targeted pathogen, thus considerably improving the pathogen capture efficiency. The uniformly distributed BP/Apt nanostructure across a large range also benefits efficient treatment of pathogen.

Bacteria Capture Performance Evaluation. To unambiguously evaluate the performance of the BP/Apt substrate and visualize the capture and release processes, we utilized *E. coli* with a red fluorescent protein gene expressing plasmid and *S. aureus* as representative pathogen models. The aptamer-modified smooth glass (glass/Apt) and BP substrates were chosen as control substrates. From the schematic and SEM images (Figure 1c and Figure S8), the *E. coli* and *S. aureus* attached on the BP/Apt surface clearly reveal the formed filopodia and stretched cell wall, while the *E. coli* maintains a smooth surface and intact cell wall on the glass/Apt substrate (Figure 1e), suggesting that the captured bacteria exhibit a strong adhesion capability and interfacial interaction with the BP/Apt substrates. In addition, as indicated in the SEM (Figure 1c and 1e) and fluorescence micrograph images (Figure 1d and 1f), in contrast with the negligible *E. coli* absorbed on the glass/Apt substrate, a significantly improved number of *E. coli* were captured by the BP/Apt substrate.

The amount of *E. coli* captured by the BP/Apt substrate increases with time, and the substrate could reach a maximum
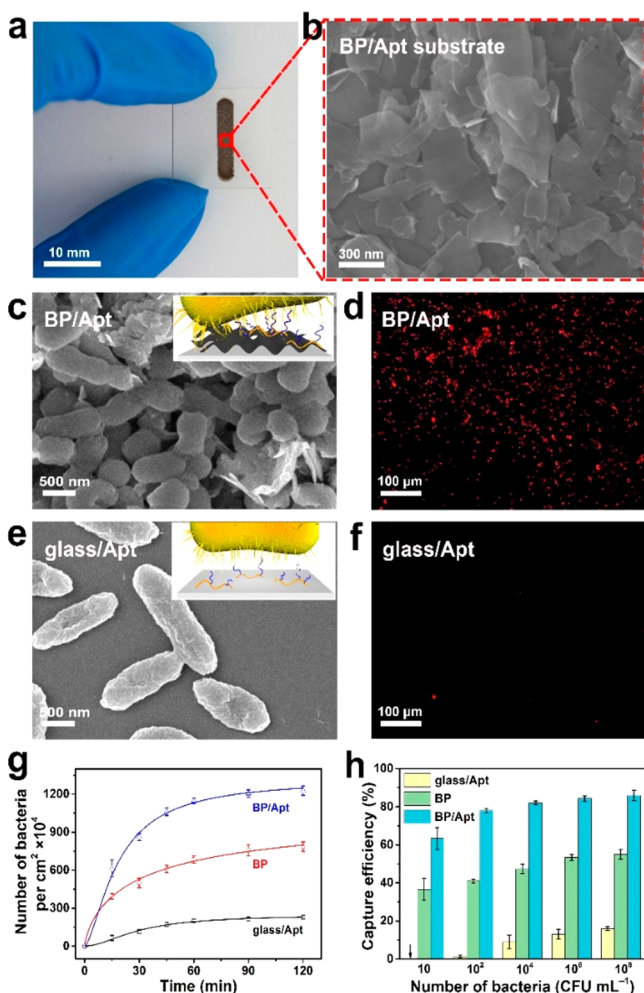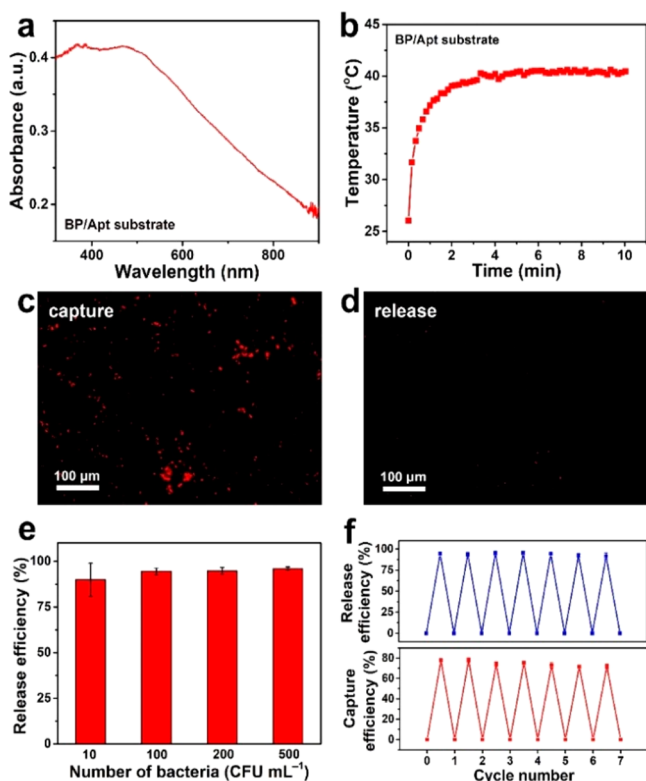
Figure 1. BP/Apt substrate for bacteria capture. (a) Photograph of the BP/Apt substrate. (b) SEM image of the BP/Apt nanostructure. Representative SEM and fluorescence images of *E. coli* with a red fluorescent protein gene expressing plasmid captured on the (c, d) BP/Apt substrate and (e, f) glass/Apt surface. (Insets of c and e) Corresponding schematic images. *E. coli* concentration is 10^8 CFU mL^{-1}. (g) *E. coli* capture numbers of glass/Apt, BP, and BP/Apt substrates as a function of incubation times. *E. coli* concentration is 10^8 CFU mL^{-1}. (h) Capture efficiency of glass/Apt, BP, and BP/Apt substrates for different concentrations of *E. coli*. In g and h, capture numbers and efficiencies were measured with three different substrates and error bars represent the standard deviations from the mean.

bacteria capture number (12.3×10^6 cells cm^{-2}) within only a 60 min incubation time (Figure 1g). Also, the number of captured *E. coli* on the BP/Apt substrate (12.3×10^6 cells cm^{-2}) is more than 5 times higher than that of glass/Apt substrate (2.3×10^6 cells cm^{-2}), indicating that the rough BP structure with improved bacteria binding affinity plays a key role in enhancing bacteria capture. On the smooth glass/Apt substrate, the capture efficiency of *E. coli* is only 16% and increases to 55% on the BP substrate with rough nanostructure (Figure 1h). The capture efficiency of the BP/Apt substrate for *E. coli* significantly increases to 86.0%, suggesting that the combination of BP nanostructure and aptamer synergistically enhances the interaction between BP/Apt substrate and pathogen and contributes to improved bacteria capture. This capture efficiency is comparable to that of reported captured substrates such as Si nanowire arrays (90%)[20] and nearly the

bendable polycrystalline $NiCo_2O_4$ nanowires (97%)[21] and is substantially higher than that of a graphene−silver nano-particle−silicon sandwich chip (54%)[22] and molecules conjugated silver nanoparticles on a silicon wafer (60%).[23] It is noted that as for our designed BP/Apt substrate prepared with a simple dip-coating strategy, the BP nanosheets are degradable and would not include additional pollution into the environment, promising its substantial potential for clinical applications. Even at relatively low *E. coli* concentrations (10 CFU mL^{-1}), the BP/Apt substrate could maintain a bacteria capture efficiency of 63% (Figure 1h), suggesting that the BP/Apt substrate exhibits extremely high sensitivity to rapidly screen a trace amount of pathogen in clinical samples due to the improved substrate/pathogen binding affinity. In addition to the *E. coli* model, a similar capture behavior was also observed when the target bacterium was *S. aureus* (Figure S9), indicating the feasibility and flexibility of the BP/Apt substrate for different clinical sample applications. To test whether the BP/Apt capture substrate is selective for a given type of pathogen, the *E. coli*-specific aptamer-conjugated BP nano-structure was exposed to a mixed sample containing *E. coli* (50%) and *S. aureus* (50%). As shown in Figure S10, the *E. coli* aptamer-modified BP substrate is 6-fold more selective for *E. coli* (capture efficiency, 78.0%) than *S. aureus* (capture efficiency, 12.3%), suggesting that the designed BP/Apt substrate could provide selectivity for targeted pathogen. The enhanced bacteria capture capability and high selectivity of the BP/Apt substrate are advantageous for clinical pathogen detection.

Photothermal Performance of the BP/Apt Substrate. The light absorption capability of the BP/Apt substrate was evaluated by the spectral measurements. The UV−vis−NIR absorption spectrum in Figure 2a demonstrates that the BP/Apt substrate exhibits high and broad spectral absorption across the measured spectrum range. To evaluate the stability of the BP-based substrate, the BP and BP/Apt substrates with the same content of BP were exposed to air for 12 days and the optical performance was recorded. As shown in Figure S11, in contrast to the sharp decrease in the spectral absorption intensity of BP substrate, the BP/Apt substrate maintains a relatively stable absorption capability during the exposure periods. In addition, there exists an observable color shallow in the optical image of BP substrate after exposing it to air for 12 days, while the BP/Apt substrate retains relatively intact in morphology and color (Figure S12). The above results indicate that the PEG conjugation isolates the BP from air and maintains the structure of BP nanosheets to some degree, thus leading to enhanced stability of the BP/Apt substrate and preventing the degradation of BP nanosheets. The excellent and stable spectral absorption of the BP/Apt substrate is beneficial for the efficient photo to thermal transfer. The surface temperature of the BP/Apt substrate was monitored with a NIR camera under NIR light irradiation (808 nm, 1 W cm^{-2}) to evaluate the photothermal performance of the BP/Apt substrate. As shown in Figure 2b and Figure S13, the surface temperature of the BP/Apt substrate quickly rises to 38 °C within 2 min and then gradually stabilizes to ~40 °C after prolonging the irradiation time to 4 min, indicating that the BP/Apt substrate could effectively convert light to heat. The temperature distribution of the BP/Apt device is uniform across the measured range, further suggesting that the BP/Apt nanosheets are uniformly distributed in the substrate. The photothermal stability of the BP/Apt substrate was also

Figure 2. NIR-responsive BP/Apt substrate for bacteria release. (a) Absorption spectra of the BP/Apt substrate across the UV−vis−NIR region. (b) Surface temperature versus irradiation time of the BP/Apt substrate irradiated with 808 nm laser (1 W cm^{-2}) for 10 min. Fluorescence images of *E. coli* with a red fluorescent protein gene expressing plasmid on the BP/Apt substrate (c) before and (d) after photothermal-triggered release. *E. coli* concentration is 10^4 CFU mL^{-1}. (e) Release efficiency of the BP/Apt substrate after capturing different spiked numbers of *E. coli* during the capture process. Error bars represent the measurements from three substrates. (f) Capture and release efficiencies of the BP/Apt substrate after recycled use for 7 cycles.

evaluated by recording the temperature curves of the BP/Apt substrate for 5 repeated NIR irradiation cycles. As shown in Figure S14, the BP/Apt substrate maintains a stable photothermal conversion performance even after five light irradiation cycles, which is attributed to the excellent photothermal performance of BP and the protection effect of PEG layers. The excellent spectral absorption and stable photothermal performance of the BP/Apt substrate is responsible for efficient pathogen release.

NIR-Mediated Release of Bacteria from the BP/Apt Substrate. Illuminating the BP/Apt substrate with NIR light triggers photothermal effects of the BP nanostructure and increases the local interface temperature to regulate the interaction forces between the bases of the aptamer,[36,37] thereby inducing the conformation change of the aptamer and leading to detachment of captured pathogen (Figure S15). As can be evidenced by the fluorescence images in Figure 2c and 2d, the number of *E. coli* exhibits a significant decrease after the release process, suggesting that the captured *E. coli* was effectively released from the substrate surface. The pathogen release efficiency was evaluated with the standard colony-counting method. It is demonstrated that the BP/Apt substrate could release pathogens without compromising the viability and integrity of the pathogens. As shown in Figure 2e, the *E.*

coli release efficiency is maintained higher than 90.0% for measured spiked cell numbers and the release efficiency reaches as high as 95.9%, suggesting the effectiveness of the BP/Apt substrate in controlled pathogen release. After releasing the captured bacteria, the structure of the aptamer is restored to the original conformation upon turning off the NIR light and the BP/Apt substrate can be used for recycled capture and release without compromising the capture and release efficiency (Figure 2f), indicating that the BP/Apt structure with a high surface roughness exhibits excellent structure durability and reproducibility for pathogen isolation and release. In addition to the *E. coli* model, a similar release capability was also observed for the *S. aureus* model when the BP/Apt substrate was modified with *S. aureus*-specific aptamer (Figure S16).

Investigation of the Performance of BP/Apt Device in Complex Environments. To validate the availability of the BP/Apt substrate for complex physiological samples, human serum was spiked with different numbers (10, 100, 200, and 500 CFU mL^{-1}) of *E. coli* and then exposed to the BP/Apt substrate. The high-efficiency capture can be confirmed by the fluorescence microscopy images of the BP/Apt substrate after *E. coli* capture (Figure 3a). The BP/Apt substrate also enables
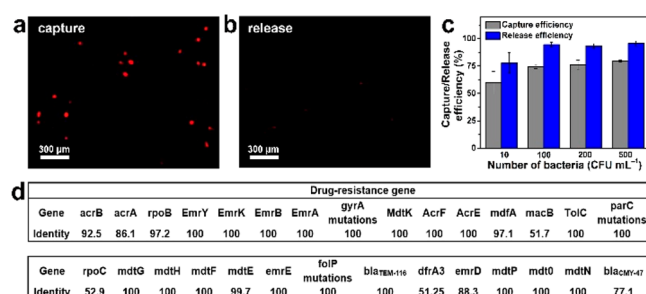
Figure 3. Availability of the BP/Apt substrate for complex biological samples treatment. (a) Fluorescence image of *E. coli* with a red fluorescent protein gene expressing plasmid captured on the BP/Apt substrate. *E. coli* was suspended in human serum samples with a concentration of 100 CFU mL^{-1}. (b) Fluorescence image of *E. coli* captured on the BP/Apt substrate after photothermal-triggered release. (c) Capture and release efficiencies of the BP/Apt substrate as a function of the number of *E. coli* spiked into human serum samples. Error bars represent the measurements from three substrates. (d) Genetic expression of released *E. coli* from the BP/Apt substrates.

efficient release of captured *E. coli* (Figure 3b). As indicated in Figure 3c, the average capture efficiencies of the BP/Apt substrate for 10, 100, 200, and 500 spiked cells mL^{-1} reach 60.0%, 74.3%, 76.3%, and 79.5%, respectively. After NIR irradiation, the BP/Apt substrate shows *E. coli* release efficiencies of 77.8%, 94.7%, 93.4%, and 95.8% for 10, 100, 200, and 500 spiked cells mL^{-1}, respectively. The capture and release efficiencies of the BP/Apt substrate for spiked *E. coli* or *S. aureus* in serum samples are comparable to those in PB buffers, indicating that the interferences in complex samples are effectively minimized (Figure 3c and Figure S17). The ability to selectively and sensitively capture pathogen out of complex biological samples illustrates the ability of the BP/Apt substrate to be applied in practical patient samples.

Genetic Analysis. In this work, we measured the complete genome sequences of released *E. coli* with known ampicillin resistance from the serum samples to investigate its antibiotic resistance. From Figure 3d, 29 antibiotic-resistant genes (>45%

identity) were identified in *E. coli*, which includes the multidrug-resistant efflux pump, multidrug efflux complex, and especially the ampicillin-resistante genes (bla$_{TEM-116}$ and bla$_{CMY-47}$). These results are consistent with the ampicillin resistance for selected *E. coli*. The downstream genetic analysis enabled by the pathogen capture/release substrate highlights the capability of the designed BP/Apt substrate for clinical investigations.

CONCLUSION

In summary, a unique strategy that uses the BP nanostructure functionalized with a temperature-sensitive aptamer for high-efficiency isolation and NIR light-mediated release of pathogen in serum is presented. With aptamer-functionalized BP nanoassemblies on the substrate as an effective tool, we are able to specifically and sensitively isolate and identify trace amounts of targeted pathogen with 86.0% capture efficiency. Furthermore, the captured bacteria could be effectively released (reaches as high as 95.9% in release efficiency) through fine tuning the structure of the aptamer with NIR light due to the photothermal effect of the BP substrate and thermal-triggered structure deformation of the aptamer. The BP/Apt substrate also shows a stable capture and release efficiency even after recycling capture and NIR light-mediated release. Notably, the BP/Apt substrate can be utilized for practical complex biological samples without compromising the excellent capture and release efficiency. The downstream genetic analysis validates the drug-resistant gene of the released pathogen, providing guidance for targeted cancer concurrent infectious diseases treatment. This proof-of-concept design was embodied for the first time and can be used in other microorganisms such as tumor cells and viruses for the purpose of targeted treatment. Although large-scale clinical studies are required to validate our approach, the high-efficiency isolation of pathogen in serum as well as controlled release of pathogen for further downstream molecular analysis provides a powerful tool toward the development of a nanotechnology platform for accurate medicine and personal healthcare.

ASSOCIATED CONTENT

ⓢ Supporting Information

The Supporting Information is available free of charge at https://pubs.acs.org/doi/10.1021/acs.analchem.0c02216.

> Experimental details; TEM images, AFM images, and Raman spectra of the BP and BP/PEG nanosheets; zeta potential of the BP, BP/PEG, and BP/Apt suspensions; elemental mapping of the BP/PEG nanosheets; SEM image of *S. aureus* captured on the BP/Apt substrate; capture and release performance estimation of the BP/Apt substrate for *S. aureus*; specificity evaluation of the BP/Apt substrate; UV−vis−NIR absorption spectra and photograph of the BP and BP/Apt substrates after exposure in air for different time intervals; photothermal cycling stability of the BP/Apt substrate under NIR irradiation; CD spectra, XPS spectra, and IR thermal image of the BP/Apt substrate; release efficiency of the BP/Apt substrate for *S. aureus*; performance evaluation of the BP/Apt substrate for *S. aureus* spiked in human serum (PDF)

AUTHOR INFORMATION

Corresponding Author

    Quan Yuan − *Key Laboratory of Analytical Chemistry for Biology and Medicine (Ministry of Education), College of Chemistry and Molecular Sciences, Wuhan University, Wuhan 430072, China; Molecular Science and Biomedicine Laboratory, State Key Laboratory of Chemo/Biosensing and Chemometrics, College of Chemistry and Chemical Engineering, Hunan University, Changsha 410082, China;* ⓞ orcid.org/0000-0002-3085-431X; Email: yuanquan@whu.edu.cn

Authors

    Yanbing Yang − *Key Laboratory of Analytical Chemistry for Biology and Medicine (Ministry of Education), College of Chemistry and Molecular Sciences, Wuhan University, Wuhan 430072, China; Key Laboratory for Micro-/Nano-Optoelectronic Devices of Ministry of Education, School of Physics and Electronics, Hunan University, Changsha 410082, China*

    Bo Zeng − *Key Laboratory of Analytical Chemistry for Biology and Medicine (Ministry of Education), College of Chemistry and Molecular Sciences, Wuhan University, Wuhan 430072, China*

    Jing Guo − *Key Laboratory of Analytical Chemistry for Biology and Medicine (Ministry of Education), College of Chemistry and Molecular Sciences, Wuhan University, Wuhan 430072, China*

    Yingxue Li − *Key Laboratory of Analytical Chemistry for Biology and Medicine (Ministry of Education), College of Chemistry and Molecular Sciences, Wuhan University, Wuhan 430072, China*

    Yujie Yang − *Key Laboratory of Analytical Chemistry for Biology and Medicine (Ministry of Education), College of Chemistry and Molecular Sciences, Wuhan University, Wuhan 430072, China*

Complete contact information is available at:
https://pubs.acs.org/10.1021/acs.analchem.0c02216

Author Contributions

§Y.B.Y. and B.Z. contributed equally to this work.

Notes

The authors declare no competing financial interest.

ACKNOWLEDGMENTS

REFERENCES

(1) June, C. H.; O'Connor, R. S.; Kawalekar, O. U.; Ghassemi, S.; Milone, M. C. *Science* **2018**, *359*, 1361−1365.

(2) Ribas, A.; Wolchok, J. D. *Science* **2018**, *359*, 1350−1355.

(3) Zhang, J. J.; Xiang, Y.; Novak, D. E.; Hoganson, G. E.; Zhu, J. J.; Lu, Y. *Chem. - Asian J.* **2015**, *10*, 2221−2227.

(4) Wang, W.; Qian, Y. C.; Li, J. H.; Aljuhani, N.; Siraki, A. G.; Le, X. C.; Li, X. F. *Environ. Sci. Technol.* **2018**, *52*, 2898−2908.

(5) Wang, F.; Liu, J. W. *Small* **2014**, *10*, 3927−3931.

(6) Zheng, F. Y.; Cheng, Y.; Wang, J.; Lu, J.; Zhang, B.; Zhao, Y. J.; Gu, Z. Z. *Adv. Mater.* **2014**, *26*, 7333−7338.

(7) Wang, S. S.; Zhao, X. P.; Liu, F. F.; Younis, M. R.; Xia, X. H.; Wang, C. *Anal. Chem.* **2019**, *91*, 4413−4420.

(8) Cao, J.; Zhao, X. P.; Younis, M. R.; Li, Z. Q.; Xia, X. H.; Wang, C. *Anal. Chem.* **2017**, *89*, 10957−10964.

(9) Yang, Y. B.; Yang, X. D.; Zou, X. M.; Wu, S. T.; Wan, D.; Cao, A. Y.; Liao, L.; Yuan, Q.; Duan, X. F. *Adv. Funct. Mater.* **2017**, *27*, 1604096.

(10) Blander, J. M.; Longman, R. S.; Iliev, I. D.; Sonnenberg, G. F.; Artis, D. *Nat. Immunol.* **2017**, *18*, 851−860.

(11) Wang, J.; Jia, H. J. *Nat. Rev. Microbiol.* **2016**, *14*, 508−522.

(12) Jin, C. C.; Lagoudas, G. K.; Zhao, C.; Bullman, S.; Bhutkar, A.; Hu, B.; Ameh, S.; Sandel, D.; Liang, X. S.; Mazzilli, S.; Whary, M. T.; Meyerson, M.; Germain, R.; Blainey, P. C.; Fox, J. G.; Jacks, T. *Cell* **2019**, *176*, 998−1013.

(13) Dejea, C. M.; Fathi, P.; Craig, J. M.; Boleij, A.; Taddese, R.; Geis, A. L.; Wu, X.; DeStefano Shields, C. E.; Hechenbleikner, E. M.; Huso, D. L.; Anders, R. A.; Giardiello, F. M.; Wick, E. C.; Wang, H.; Wu, S.; Pardoll, D. M.; Housseau, F.; Sears, C. L. *Science* **2018**, *359*, 592−597.

(14) Roope, L. S. J.; Smith, R. D.; Pouwels, K. B.; Buchanan, J.; Abel, L.; Eibich, P.; Butler, C. C.; Tan, P. S.; Walker, A. S.; Robotham, J. V.; Wordsworth, S. *Science* **2019**, *364*, No. eaau4679.

(15) Peng, B.; Zhang, X. L.; Aarts, D. G. A. L.; Dullens, R. P. A. *Nat. Nanotechnol.* **2018**, *13*, 478−482.

(16) Stokes, J. M.; Gutierrez, A.; Lopatkin, A. J.; Andrews, I. W.; French, S.; Matic, I.; Brown, E. D.; Collins, J. J. *Nat. Methods* **2019**, *16*, 303−306.

(17) Etayash, H.; Khan, M. F.; Kaur, K.; Thundat, T. *Nat. Commun.* **2016**, *7*, 12947−12955.

(18) Sang, Y. J.; Li, W.; Liu, H.; Zhang, L.; Wang, H.; Liu, Z. W.; Ren, J. S.; Qu, X. G. *Adv. Funct. Mater.* **2019**, *29*, 1900518−1900527.

(19) Chen, Z. Y.; Mo, M.; Fu, F. F.; Shang, L. R.; Wang, H.; Liu, C. H.; Zhao, Y. J. *ACS Appl. Mater. Interfaces* **2017**, *9*, 38901−38907.

(20) Li, Y. Q.; Zhu, B. W.; Li, Y. G.; Leow, W. R.; Goh, R.; Ma, B.; Fong, E.; Tang, M.; Chen, X. D. *Angew. Chem., Int. Ed.* **2014**, *53*, 5837−5841.

(21) Fang, C. H.; Shao, L.; Zhao, Y. H.; Wang, J. F.; Wu, H. K. *Adv. Mater.* **2012**, *24*, 94−98.

(22) Liu, L. Z.; Chen, S.; Xue, Z. J.; Zhang, Z.; Qiao, X. Z.; Nie, Z. X.; Han, D.; Wang, J. L.; Wang, T. *Nat. Commun.* **2018**, *9*, 444−452.

(23) Mao, S.; Chang, J. B.; Pu, H. H.; Lu, G. H.; He, Q. Y.; Zhang, H.; Chen, J. H. *Chem. Soc. Rev.* **2017**, *46*, 6872−6904.

(24) Xu, Y. S.; Wang, H.; Luan, C. X.; Liu, Y. X.; Chen, B. A.; Zhao, Y. J. *Biosens. Bioelectron.* **2018**, *100*, 404−410.

(25) Meng, X. Y.; Wang, H. Y.; Chen, N.; Ding, P.; Shi, H. Y.; Zhai, X.; Su, Y. Y.; He, Y. *Anal. Chem.* **2018**, *90*, 5646−5653.

(26) Zhao, Y. T.; Tong, L. P.; Li, Y.; Pan, H. B.; Zhang, W.; Guan, M.; Li, W. H.; Chen, Y. X.; Li, Q.; Li, Z. J.; Wang, H. Y.; Yu, X. F.; Chu, P. K. *ACS Appl. Mater. Interfaces* **2016**, *8*, 5813−5820.

(27) Wang, H. Y.; Zhou, Y. F.; Jiang, X. X.; Sun, B.; Zhu, Y.; Wang, H.; Su, Y. Y.; He, Y. *Angew. Chem., Int. Ed.* **2015**, *54*, 5132−5136.

(28) Zhuang, J. L.; Wu, Y. J.; Chen, L.; Liang, S. P.; Wu, M. H.; Zhou, L. D.; Fan, C. H.; Zhang, Y. Q. *Adv. Sci.* **2018**, *5*, 1801158.

(29) Chen, G. Y.; Agren, H.; Ohulchanskyy, T. Y.; Prasad, P. N. *Chem. Soc. Rev.* **2015**, *44*, 1680−1713.

(30) Kundu, P. K.; Samanta, D.; Leizrowice, R.; Margulis, B.; Zhao, H.; Borner, M.; Udayabhaskararao, T.; Manna, D.; Klajn, R. *Nat. Chem.* **2015**, *7*, 646−652.

(31) Zhao, J.; Chu, H. Q.; Zhao, Y.; Lu, Y.; Li, L. L. *J. Am. Chem. Soc.* **2019**, *141*, 7056−7062.

(32) Chen, W. S.; Ouyang, J.; Liu, H.; Chen, M.; Zeng, K.; Sheng, J. P.; Liu, Z. J.; Han, Y. J.; Wang, L. Q.; Li, J.; Deng, L.; Liu, Y. N.; Guo, S. J. *Adv. Mater.* **2017**, *29*, 1603864−1603870.

(33) Zhou, W. H.; Pan, T.; Cui, H. D.; Zhao, Z.; Chu, P. K.; Yu, X. F. *Angew. Chem., Int. Ed.* **2019**, *58*, 769−774.

(34) Yang, B. W.; Yin, J. H.; Chen, Y.; Pan, S. S.; Yao, H. L.; Gao, Y. S.; Shi, J. L. *Adv. Mater.* **2018**, *30*, 1705611−1705622.

(35) Shen, H. J.; Wang, J.; Liu, H. Y.; Li, Z. H.; Jiang, F. L.; Wang, F. B.; Yuan, Q. *ACS Appl. Mater. Interfaces* **2016**, *8*, 19371−19378.

(36) Wang, J.; Wei, Y. R.; Hu, X. X.; Fang, Y. Y.; Li, X. Y.; Liu, J.; Wang, S. F.; Yuan, Q. *J. Am. Chem. Soc.* **2015**, *137*, 10576−10584.

(37) Cai, S. D.; Yan, J. H.; Xiong, H. J.; Liu, Y. F.; Peng, D. M.; Liu, Z. B. *Analyst* **2018**, *143*, 5317−5338.